Chapter 7

Use of Bio-Layer Interferometry (BLI) to Measure Binding Affinities of SNAREs and Phosphoinositides

Jorge D. Calderin, Chi Zhang, Timothy J. C. Tan, Nicholas C. Wu, and Rutilio Fratti

Abstract

Bio-Layer Interferometry (BLI) is a technique that uses optical biosensing to analyze interactions between molecules. The analysis of molecular interactions is measured in real-time and does not require fluorescent tags. BLI uses disposable biosensors that come in a variety of formats to bind different ligands including biotin, hexahistidine, GST, and the Fc portion of antibodies. Unlike surface plasmon resonance (SPR), BLI is an open system that does not require microfluidics, which eliminates issues that result from clogging and changes in viscosity. Importantly, BLI readings can be completed in minutes and can be formatted for high throughput screening. Here we use biotinylated short chain phosphoinositides and phosphatidic acid bound to streptavidin BLI biosensors to measure the binding of the soluble Qc SNARE Vam7 from *Saccharomyces cerevisiae*. Unlike most SNAREs, Vam7 lacks a transmembrane domain or lipid anchor to associate with membranes. Instead Vam7 associates to yeast vacuolar membranes using its N-terminal PX domain that binds to phosphatidylinositol 3-phosphate (PI3P) and phosphatidic acid (PA). Using full length Vam7, Vam7^{Y42A}, and PX domain alone, we determined and compared the dissociation constants (K_D) of each to biotinylated PI3P and PA biosensors.

Key words Phosphatidylinositol, Phosphatidic acid, PX, Vam7, SNARE

1 Introduction

Molecule transport between eukaryotic organelles occurs through the fusion of two membranes into a continuous bilayer allowing the transfer of cargo. The fusion of these membranes requires a conserved set of proteins and lipids that regulate a series of experimentally defined stages culminating in the use of SNARE proteins to form complexes between membranes to trigger fusion [1, 2].

Membranes contain bulk lipids including phosphatidylcholine, phosphatidylserine, and phosphatidylethanolamine, as well as a group of regulatory lipids that are low in abundance but have a large influence on membrane fusion. These include phosphatidic acid (PA), diacylglycerol (DAG) and a set of differentially

Rutilio Fratti (ed.), *SNAREs: Methods and Protocols*, Methods in Molecular Biology, vol. 2887,
https://doi.org/10.1007/978-1-0716-4314-3_7,

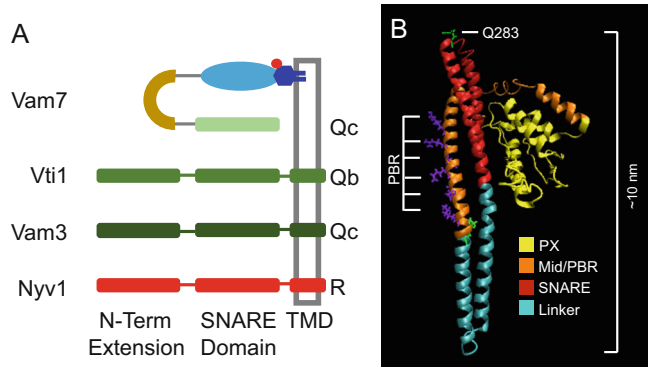

Fig. 1 Schematic of vacuolar SNAREs and computation model of Vam7. (**a**) Shown are the SNARE required for vacuole homotypic fusion. The Q-SNAREs Vam3, Vti1 and the R-SNARE Nyv1 have N-terminal extensions, a SNARE domain and transmembrane domains that pass through the vacuole membrane. The Q-SNARE Vam7 has an N-terminal PX domain that binds the membrane through binding PI3P followed by a Mid domain and a C-terminal SNARE domain. (**b**) A structural prediction of Vam7 determined by Phyre2 and visualized with VMD. A similar structure was predicted by alpha-fold

phosphorylated phosphoinositides (PI), e.g., PI 3-phosphate (PI3P) and PI(3,5)P_2 [3–18]. Yeast vacuole fusion requires these regulatory lipids as well as their interconversion by phosphatases, kinases, and lipases. The function of regulatory lipids in vacuole fusion mostly occurs through direct interaction with proteins including the yeast vacuolar SNARE Vam7 [2, 19].

In *Saccharomyces cerevisiae*, vacuoles/lysosomes undergo rounds of fission and homotypic fusion throughout the cell cycle and as a response to stress, including osmotic shock [20, 21]. Vacuole homotypic fusion requires the Q-SNAREs Vam3, Vti1 and Vam7, and the R-SNARE Nyv1 (Fig. 1a) [22]. Unlike other SNAREs Vam7 lacks a transmembrane domain and any lipid anchors to insert into the vacuole membrane [23]. Instead Vam7 associates with membranes via its N-terminal PX (phox homology) domain that binds PI3P, PA and the HOPS tethering complex [11, 17, 24]. Structural predictions show that the PX domain folds over the SNARE domain and the linker between the SNARE and Mid domains to form a closed conformation reminiscent of the H_{abc} domain folding over the SNARE domain in Synatxin homologs (Fig. 1b) [25].

The interaction between the Vam7 PX domain and lipids has only been characterized for binding PI3P and binding to PA has only been modeled (our unpublished data) [24]. The Tyr at position 42 is essential for PI3P binding as mutating it to Ala (Y42A) completely blocks the interaction. That said, this was determined with the PX domain alone using lipid overlay assays, and NMR with dibutanoyl PI3P. Liposome binding with full-length Vam7 shows

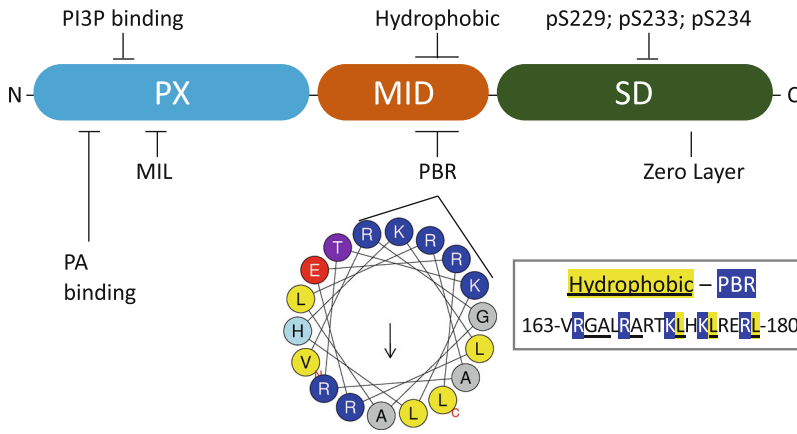

Fig. 2 Schematic of Vam7 domains and interactions. Shown is a linear representation of Vam7 and its three domains. Each domain is labeled with known interactions and features. The PX domain has binding sites for PI3P and PA as well as a membrane insertion loop. The Mid domain has an amphipathic helix where the hydrophilic side contains a polybasic region (PBR). The SNARE domain (SD) with the Zero-layer glutamine and putative phosphorylation sites. Below is a helical wheel showing the PBR and hydrophobic sites of Mid domain helix

additional interactions with PA [11, 26]. This is not unusual as PX domains have been found to bind multiple lipids through separate binding sites [27–29]. The Vam7 PX domain also has a hydrophobic membrane insertion loop (MIL) that penetrates the bilayer to enhance lipid binding [30]. Between the PX and C-terminal SNARE domains, Vam7 has a middle domain (Mid) that modulates the PI3P binding ability of the PX domain (Fig. 2) [11]. The Mid domain contains a polybasic region (PBR) with a stretch of Arg and Lys residues and mutating them to Ala results in the enhanced binding of PI3P by the neighboring PX domain. The mechanism responsible for this remains unclear. Thus, it is important to measure how Vam7 differentially binds to lipids versus mutants or the PX domain alone.

There is a variety of methods to study protein-lipid interactions to determine dissociation constants (K_D). Techniques such as Surface Plasmon Resonance (SPR), Microscale Thermophoresis (MST), isothermal titration calorimetry (ITC), and enzyme-linked immunosorbent assay (ELISA) have been used to determine binding affinities and other kinetic and thermodynamic measurements. Often, there are limitations in using these methods, including the need for large quantities of purified protein and the need for membranes to examine integral proteins. Although some techniques such as MST can accommodate low protein concentrations and membrane proteins, they may require labeling with a fluorophore, which itself can introduce unintended effects on binding. For instance, maleimide dyes require free surface exposed Cys that could be essential for function as seen with Sec18, the yeast

homolog of NSF—*N*-ethylmaleimide sensitive factor [31]. Other dyes require primary amines which would inhibit the effect of the PBR on the PX domain. Such limitations require the insertion of a free Cys, or a polyhistidine tag that binds to a Ni-NTA dye, which itself could alter protein function. An alternative for proteins that cannot be tagged at either terminus is the use of the intrinsic fluorescence of aromatic residues; however, this requires that binding between molecules does not affect the emission intensities these residues. Other limitations include the need for strenuous microfluidic tubing that requires loading optimization steps, along with the risk of clogging, as seen in methods like SPR [32–34]. One leading application that minimizes many of these drawbacks seen in other techniques is Biolayer Interferometry (BLI), which relies on biosensors like in SPR but removes the need for microfluidics and excessive washing steps, in addition to minimizing nonspecific binding artifacts through its unique "Dip and Read" approach.

Being label-free, BLI relies on measuring the interference pattern, of reflected white light from its two distinct fiber-optic biosensors, one of which contains one of the binding pairs being studied immobilized onto the sensor itself, through methods such as streptavidin-biotin interactions [34]. Before any kinetic measurements, the biosensors are incubated in wells of a pre-loaded 96-well plate designated solely for the given running buffer to create a baseline reading. Then a loading step introduces the biosensors to the ligand to be immobilized on the sensors. Following the immobilization of one of the binding pairs, an additional baseline of the ligand-immobilized biosensor in buffer conditions is measured to generate an underlining interference pattern. Protein-ligand kinetics are then measured as the biosensors are lowered into following wells containing the analyte in buffer solution; as the thickness of the immobilized biosensor changes through analyte-immobilized layer interactions, the interference pattern shifts positively, correlating to association of the binding pair [33]. After the association step, the sensors are moved into wells containing only buffer; as the analyte dissociates from its binding pair, the thickness of the sensor will decrease correlating to the dissociation of the complex which is detected as a negative shift of the interference pattern [33, 35]. This "Dip and Read" approach allows for further prevention of experimental artifacts since only analyte binding to the immobilized ligand on the biosensor can change the interference pattern, other experimental factors such as unbound protein, pH changes, and refractive index will not be detrimental to the kinetic results. The less restrictive parameters of BLI allow interactions to be tested without the need for excessive volumes while also not consuming samples throughout the process, allowing for the possibility of sample recovery.

In this protocol, we used the Octet RED96e FortéBIO system that utilizes 96-well microplates throughout its screenings, allowing the BLI approach to increase scalability of samples and conditions compared to other applications [34]. This scalability allows for kinetic screenings with various concentrations of ligand to occur simultaneously for accurate and time-efficient kinetic results. Furthermore, the use of 96 well plates, and running simultaneous kinetics assays, allows for the comparison of competitive binding pairs, as multiple analytes can be tested against the same ligand-immobilized biosensors.

The advancements and simplicities of BLI to measure protein-ligand binding kinetics have resulted in the technique emerging in numerous other studies. Research into furthering the capabilities of BLI has also shown that it can measure binding kinetics beyond just protein-protein and protein-ligand interactions but can measure binding kinetics between immobilized protein and liposomes in solution, giving further insights into how proteins, and potential drugs, may be interacting with their membrane-embedded binding targets [33].

2 Materials

2.1 Reagents

1. 1 M Tris-Cl, pH 8 (*see* **Note 1**)
2. 5 M NaCL
3. Isopropyl-1-thio-β-D-galactopyranoside (IPTG)
4. 1 M Dithiothreitol (DTT)
5. 0.2 M Ethylenediaminetetraacetic acid (EDTA)
6. 0.2 M Ethylene glycol-bis(β-aminoethyl ether)-N,N,N′,N′ tetraacetic acid (EGTA)
7. Bradford reagent
8. 2× Laemmli SDS-PAGE sample buffer
9. Coomassie Blue
10. Precast 10% polyacrylamide gel
11. PIPES-Sorbitol (PS) Buffer: 20 mM PIPES-KOH, pH 6.8, 200 mM Sorbitol
12. Phosphate-buffered saline (PBS): 137 mM NaCl, 2.5 mM KCl, 10 mM NaH_2PO_4, 2 mM KH_2PO_4, pH 7.4
13. Running BLI Buffer: PBS with 0.002% Tween-20 (v/v) (*see* **Note 2**)
14. Biotinylated Phosphatidylinositol 3-phosphate (b-PI3P): 10 μg b-PI3P (MW: 1030.9 g/mL) dissolved in 97 mL PS Buffer for a final concentration of 0.1 μM.

15. Biotinylated Phosphatidic acid (b-PA): 10 μg b-PA (MW: 836.09 g/mol) dissolved in 119.6 mL PS Buffer for a final concentration of 0.1 μM.
16. Black and flat bottom Greiner Bio 96 Well Microplate
17. Avidin BLI biosensor

2.2 Protein Purification

1. Luria broth (LB) and agar plates with kanamycin or kanamycin and chloramphenicol
2. Terrific broth (TB) with kanamycin or kanamycin and chloramphenicol
3. pET42a(+) plasmid
4. *Escherichia coli* Rosetta 2 (DE3) pLysS competent cells
5. *E. coli* DH5α competent cells
6. Protease inhibitors: phenylmethylsulfonyl fluoride (PMSF); Pefabloc-SC, Leupetin, Pepstatin.
7. Lysis buffer: 50 mM Tris-Cl pH 8, 500 mM NaCl, 1 mM DTT, 2 mM EGTA, 1 mM EDTA, 1 mM PMSF, 10 μM Pefabloc-SC, 1 μM leupeptin, 5 μM pepstatin. (*see* **Note 3**)
8. Elution buffer: Lysis buffer with 10 mM reduced glutathione
9. Glutathione resin (*see* **Note 4**)

2.3 Equipment

1. PCR machine
2. Beckman ultracentrifuge with Type 70-Ti rotor or similar
3. Nutator
4. Octet Red 96e FortéBIO System

3 Methods

3.1 Plasmid Construction and Protein Purification

1. Amplify full-length Vam7 and the PX domain from *S. cerevisiae* BY4742 genomic DNA by PCR, using forward primer 5′ GCG**GGATCC**GCAGCTAATTCTGTAGGGAAA-3′ with a BamHI restriction site (bold) and reverse primer 5′ CGC**GAATTC**TCAAGCACTGTTGTTAAAATG-3′ with an EcoRI site (bold) as described [36, 37]. For the PX domain (aa 2–125), use the forward primer from above and the reverse primer 5′-CGC**GAATTC** CTATCAAACATTTGGCTTTGA CAACTG′-3 with an EcoRI site (bold). Make Vam7^{Y42A} by QuickChange mutagenesis with forward primer 5′-AACAAG CGCCTTTACAAAAGGGCATCCGAGTTTTGGAAACT GAAG -3′ and reverse primer 5′-CTTCAGTTTCCAAAACTCGGATGCCCTTTTG TAAAGGCGCTTGTT-3′.

2. Digest the amplicons and ligate to BamH1/Eco1 linearized pET42a(+) plasmid to be under the control of the T7 promoter. Then transform into DH5α *E. coli* using standard methods (*see* **Note 5**).
3. Verify the correct sequences of the GST-Vam7/PX fusions.
4. Transform pET42a-GST-Vam7/PX constructs into *E. coli* Rosetta-2 (DE3) pLysS and grow on LB with kanamycin and chloramphenicol (*see* **Note 6**).
5. For recombinant expression, inoculate 2 L of Terrific broth for each construct and grow to $A_{600} = 0.6$ at 37 °C in a shaking incubator.
6. Induce expression by adding 500 μM IPTG and incubate for 4 h at 37 °C while shaking (*see* **Note 7**).
7. Harvest cells by centrifugation and wash twice with lysis buffer then lyse by three passes through French pressure cell.
8. Clarify the lysate by ultracentrifugation at 203,347× *g* (45,000 rpm) for 60 min at 4 °C in a Type 60 Ti rotor.
9. Equilibrate 3 mL glutathione resin with 20 column volumes of lysis buffer.
10. Collect supernatant and incubate with equilibrated glutathione resin for 16 h at 4 °C while nutating (*see* **Note 8**).
11. Collect flowthrough.
12. Wash resin with 20 column volumes of lysis buffer.
13. Release GST-Vam7 with elution buffer in 0.5 mL fractions.
14. Test for protein by mixing 10 μL of each fraction with 200 μL Bradford reagent. Save 10 μL of each fraction with a strong protein signal and mix with 10 μL 95 °C 2× SDS loading buffer and boil for 5 min.
15. Resolve fractions by SDS-PAGE and stain with Coomassie Blue to visualize proteins.
16. Pool Vam7 protein peak and dialyze overnight against PS buffer with 125 mM KCl and 5 mM $MgCl_2$ at 4 °C using a magnetic stirrer.
17. Aliquot protein (50 μL) in 0.5 ml microcentrifuge tubes and flash freeze in liquid nitrogen. Store at −80 °C (*see* **Note 9**).

3.2 Pre-loading 96-Well Plate and Sample Preparation

1. Resuspend biotin-labeled lipids in PS buffer to a final concentration of 0.1 μM.
2. Dilute to 500 nM with BLI running buffer
3. Load 190 μL of 500 nM biotin-labeled lipids (PI3P and PA) to wells in a 96-well microplate (Fig. 3) (*see* **Note 10**).

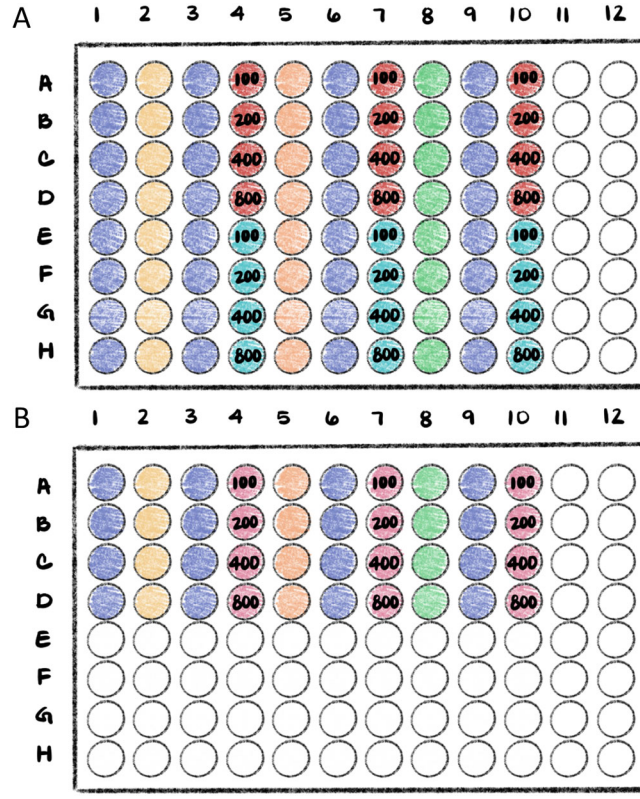

Fig. 3 Arrangement of wells for BLI measurements. (**a**) Orientation for the 96-well plate for GST-Vam7, and GST-Vam7^{Y42A} kinetic trials, blue represents BLI running buffer, yellow for 500 nM bPI(3)P and green for 500 nM bPA (*see* **Note 10**). Red wells represent analyte concentrations of 100, 200, 400, and 800 nM for GST-Vam7, whereas cyan represents similar concentrations for GST-Vam7^{Y42A}. (**b**) The blue, yellow, orange, and green wells are identical to Fig. 2a, whereas the pink color represents analyte concentrations of 100, 200, 400, and 800 nM of GST-PX

4. Since each Analyte will be screened with three different immobilized biosensors (PI3P and PA), at 4 concentrations make 2 mL of each dilution.
5. Dilute GST-PX, GST-Vam7, and GST-Vam7^{Y42A} to 100, 200, 400, and 800 nM with BLI Running Buffer.
6. 190 μL of each dilution, for each analyte, were loaded to corresponding wells (*see* **Note 11**).

3.3 Preparation of BLI Octet System

1. Hydrate biosensors in BLI running buffer for a minimum of 10 min before use (*see* **Note 12**).
2. Place the hydrated sensor rack, and pre-loaded 96-well plate in designated areas in the Octet RED96e FortéBIO system.
3. Close the hatch after placing the trays.

4. Click “Experiment” followed by “New-Experiment Wizard” and “Blank Experiment”.
5. Click “Plate Definition”: Plate definition is for highlighting the specific wells in the pre-loaded 96-well plate that will be used and tested throughout the given experiment run. Each run consists of 1 immobilized biosensor being incubated with a given analyte. As an example, for a b-PI3P experiment only use columns 1, 2, 3, and 4 (*see* **Note 13**).
6. Click “Assay Definition” followed by “Add”. Specify which columns will be used.
7. Set the protocol to shake speed (1000 rpm) for each step: Baseline (60 s), Loading (120 s), Association (180 s), and Dissociation (180 s).
8. Assign a column for each corresponding step. As an example, for the bPI(3)P experiment, Column 1 was Initial Baseline, Column 2 was Loading, Column 3 was second Baseline, Column 4 was Association, and Column 3 was used again for Dissociation.
9. Choose which sensors in the biosensor rack will be used throughout the given experiment. It’s beneficial to align your biosensor rack and 96-plate well rack similarly for easy sensor-well assignment
10. Unclick “Replace Sensors”. Used sensors will be ejected into the waste tray.
11. Run Experiment: Unclick “Delayed experiment start” and click “Shake sample plate while waiting”. Unclick “set plate temperature”, since the assays are run at room temperature.
12. Make sure “Open runtime charts automatically”, and “Automatically save runtime chart” are both clicked.
13. Press “Go” to begin the Assay.

3.4 Data Acquisition

1. After the assay has been completed, search and select the most recent data file for analysis. The sensorgram will be separated for each step throughout the assay: Baseline, Loading, Baseline, Association, and Dissociation correlating to steps assigned during step Subheading 3.3, **step 7**.
2. Click “Align Y-Axis”, “Align to Baseline”, and make sure that “Savitzky-Golay Filtering” is clicked as well. This will assist in reducing noise as the data processes.
3. Finally click the button “Process Data!” to apply conditions and proceed with data analysis.

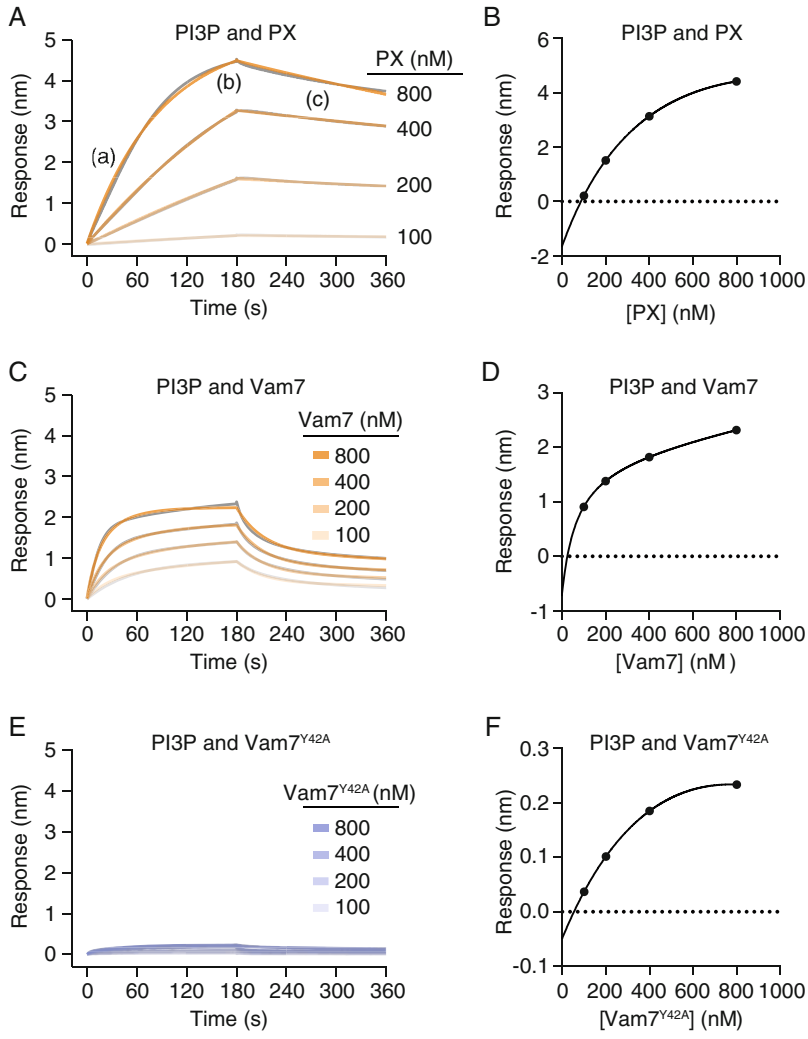

Fig. 4 Interactions between Vam7 and PI3P. PI3P binding to PX (**a**, **b**), Vam7 (**c**, **d**) and Vam7^{Y42A} (**e**, **f**), respectively. (**a**, **c**, **e**) Sensorgrams and response units over time (s) of binding to 500 nM PI3P. (**b**, **d**, **f**) BLI-determined binding affinity for PI3P binding

3.5 Analysis

1. Set a designating color, and name for analyte and immobilized-binding pair (*see* **Note 14**).
2. To analyze binding models, click the option for "Association and Dissociation", and find a model that fits best with the current sensorgram data (*see* **Note 14**). Click "Global Full" and "Group by color", which will re-group data points by the color designated in **step 1.**
3. Then click the button "Fit Curves!" and export both fitted curves and raw data results to a designated folder.

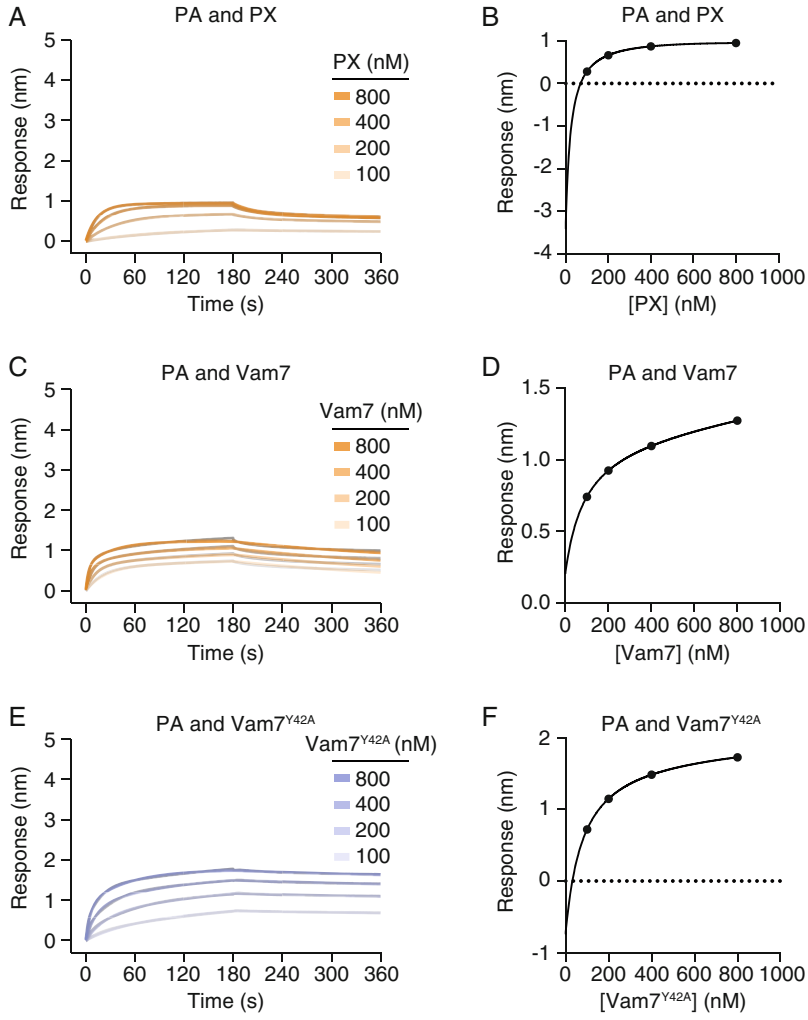

Fig. 5 Interactions between Vam7 and PA. PA binding to PX (**a**, **b**), Vam7 (**c**, **d**) and Vam7^{Y42A} (**e**, **f**), respectively. (**a**, **c**, **e**) Sensorgrams and response units over time (s) of binding to 500 nM PA. (**b**, **d**, **f**) BLI-determined binding affinity for PA binding

4. Sensorgrams are generated showing binding of PX domain, full length Vam7 and Vam7^{Y42A} to PI3P (Fig. 4) and PA (Fig. 5). Each sensorgram shows the association rate (a), steady state binding (b), and dissociation (c) of each protein concentration binding to 500 nM lipid.
5. Use steady state data to plot curves used to determine K_D values for each protein-lipid interaction (Table 1).

Table 1
Dissociation constants

Protein	K_{D1} (M)	K_{D1} error (M)	K_{D2} (M)	K_{D2} error (M)
PX + PA	9.33E-05	1.41E-04	7.08E-09	2.08E-10
Vam7 + PA	9.06E-09	3.24E-12	<1.0E-12	2.83E-09
$Vam7^{Y42A}$ + PA	<1.0E-12	7.06E-09	3.60E-09	9.34E-10
PX + PI3P	1.08E-07	4.49E-09	8.67E-08	7.73E-09
Vam7 + PI3P	1.28E-08	9.00E-12	<1.0E-12	3.12E-08
$Vam7^{Y42A}$ + PI3P	<1.0E-12	<1.0E-12	<1.0E-12	3.37E-09

4 Notes

1. 1 M Tris-HCl base becomes very cold, which will shift the pH. Instead, allow the solution to warm to room temperature before adjusting the pH.
2. 0.002% Tween-20 is used to assist in decreasing nonspecific binding interactions and artifacts.
3. Add PMSF to buffers right before use because it becomes inactive over time.
4. Glutathione resin can become oxidized over time, which will prevent binding of GST-tagged proteins. If binding fails, you can reactivate the resin with DTT.
5. The T7 promoter in pET42a lowers background expression of target genes. Plasmids with other promoters such as the Tac promoter are sufficiently leaky to accumulate Vam7, which is toxic to *E. coli* DH5α and can lead to random point mutations to occur.
6. Rosetta-2 (DE3) pLysS cells express t-RNAs for seven rare codons to improve heterologous expression. The pLysS lysozyme further lowers background expression of the target gene. Perform a fresh transformation each time you express Vam7.
7. Longer expression times result in the accumulation of degradation products. This is not helped by expression at lower temperatures.
8. Overnight binding is done for convenience and shorter periods of binding are sufficient. Binding at room temperature can be done in 1 h.
9. Vam7 is not stable for long periods of time at 4 °C and will lose activity if refrozen. To ensure maximum activity, thaw an aliquot of frozen Vam7 shortly before starting an assay. Do no refreeze leftover protein.

10. Using blank 96-well plate printouts, with written orientation of wells to help organize pre-loading and pipetting is highly recommended since correct loading is critical for BLI assays to be run correctly.
11. 96-well plate outline and orientation (Fig. 3).
12. Biosensors can be left hydrating throughout the time of plate orientation and loading, which will allocate more than enough time for hydrating the plate, 10 min is just a strict minimum. We have left 96 well plates hydrated for up to 1 h prior to use.
13. As an example, for the b-PI3P experiment, GST-Vam7 runs were designated with one color, and GST-Vam7^{Y42A} was designated with another since the runs were run simultaneously.
14. Checking R^2 values for various models can assist in finding one that first the kinetic data the best/most accurately.

Acknowledgments

This work was supported in part by National Science Foundation MCB 1818310 and MCB 2216742 (RAF), the National Institutes of Health Directors New Innovator Award DP2 AT011966 (NCW), and the Searl Scholars Program (NCW). JDC was partially supported by an NIGMS-NIH Chemistry-Biology Interface Training Grant 5 T32-GM070421.

References

1. Bonifacino JS, Glick BS (2004) The mechanisms of vesicle budding and fusion. Cell 116: 153–166. https://doi.org/10.1016/s0092-8674(03)01079-1
2. Starr ML, Fratti RA (2019) The participation of regulatory lipids in vacuole homotypic fusion. Trends Biochem Sci 44:546–554. https://doi.org/10.1016/j.tibs.2018.12.003
3. Boeddinghaus C, Merz AJ, Laage R, Ungermann C (2002) A cycle of Vam7p release from and PtdIns 3-P-dependent rebinding to the yeast vacuole is required for homotypic vacuole fusion. J Cell Biol 157:79–89. https://doi.org/10.1083/jcb.200112098
4. Cabrera M, Nordmann M, Perz A et al (2014) The Mon1-Ccz1 GEF activates the Rab7 GTPase Ypt7 via a longin-fold-Rab interface and association with PI3P-positive membranes. J Cell Sci 127:1043–1051. https://doi.org/10.1242/jcs.140921
5. Fratti RA, Jun Y, Merz AJ et al (2004) Interdependent assembly of specific regulatory lipids and membrane fusion proteins into the vertex ring domain of docked vacuoles. J Cell Biol 167:1087–1098. https://doi.org/10.1083/jcb.200409068
6. Jun Y, Fratti RA, Wickner W (2004) Diacylglycerol and its formation by phospholipase C regulate Rab- and SNARE-dependent yeast vacuole fusion. J Biol Chem 279:53186–53195. https://doi.org/10.1074/jbc.M411363200
7. Karunakaran S, Fratti RA (2013) The lipid composition and physical properties of the yeast vacuole affect the hemifusion-fusion transition. Traffic 14:650–662. https://doi.org/10.1111/tra.12064
8. Kato M, Wickner W (2001) Ergosterol is required for the Sec18/ATP-dependent priming step of homotypic vacuole fusion. EMBO J 20:4035–4040. https://doi.org/10.1093/emboj/20.15.4035
9. Lawrence G, Brown CC, Flood BA et al (2014) Dynamic association of the PI3P-interacting Mon1-Ccz1 GEF with vacuoles is controlled through its phosphorylation by the type

1 casein kinase Yck3. Mol Biol Cell 25:1608–1619. https://doi.org/10.1091/mbc.E13-08-0460

10. Mayer A, Scheglmann D, Dove S et al (2000) Phosphatidylinositol 4,5-bisphosphate regulates two steps of homotypic vacuole fusion. Mol Biol Cell 11:807–817. https://doi.org/10.1091/mbc.11.3.807
11. Miner GE, Starr ML, Hurst LR et al (2016) The central polybasic region of the soluble SNARE (soluble N-Ethylmaleimide-sensitive factor attachment protein receptor) Vam7 affects binding to phosphatidylinositol 3-phosphate by the PX (Phox homology) domain. J Biol Chem 291:17651–17663. https://doi.org/10.1074/jbc.M116.725366
12. Miner GE, Starr ML, Hurst LR, Fratti RA (2017) Deleting the DAG kinase Dgk1 augments yeast vacuole fusion through increased Ypt7 activity and altered membrane fluidity. Traffic 18:315–329. https://doi.org/10.1111/tra.12479
13. Miner GE, Sullivan KD, Zhang C et al (2020) Phosphatidylinositol 3,5-bisphosphate regulates Ca2+ transport during yeast vacuolar fusion through the Ca2+ ATPase Pmc1. Traffic 21:503–517. https://doi.org/10.1111/tra.12736
14. Zhang C, Feng Y, Balutowski A et al (2022) The interdependent transport of yeast vacuole Ca2+ and H+ and the role of phosphatidylinositol 3,5-bisphosphate. J Biol Chem 102672: 102672. https://doi.org/10.1016/j.jbc.2022.102672
15. Starr ML, Hurst LR, Fratti RA (2016) Phosphatidic acid sequesters Sec18p from cis-SNARE complexes to inhibit priming. Traffic 17:1091–1109. https://doi.org/10.1111/tra.12423
16. Starr ML, Sparks RP, Arango AS et al (2019) Phosphatidic acid induces conformational changes in Sec18 protomers that prevent SNARE priming. J Biol Chem 294:3100–3116. https://doi.org/10.1074/jbc.RA118.006552
17. Stroupe C, Collins KM, Fratti RA, Wickner W (2006) Purification of active HOPS complex reveals its affinities for phosphoinositides and the SNARE Vam7p. EMBO J 25:1579–1589. https://doi.org/10.1038/sj.emboj.7601051
18. Sasser T, Qiu Q-S, Karunakaran S et al (2012) Yeast lipin 1 orthologue pah1p regulates vacuole homeostasis and membrane fusion. J Biol Chem 287:2221–2236. https://doi.org/10.1074/jbc.M111.317420
19. Lemmon MA (2008) Membrane recognition by phospholipid-binding domains. Nat Rev Mol Cell Biol 9:99–111. https://doi.org/10.1038/nrm2328
20. Jin Y, Weisman LS (2015) The vacuole/lysosome is required for cell-cycle progression. elife 4. https://doi.org/10.7554/eLife.08160
21. Li SC, Kane PM (2009) The yeast lysosome-like vacuole: endpoint and crossroads. Biochim Biophys Acta 1793:650–663. https://doi.org/10.1016/j.bbamcr.2008.08.003
22. Wickner W (2010) Membrane fusion: five lipids, four SNAREs, three chaperones, two nucleotides, and a Rab, all dancing in a ring on yeast vacuoles. Annu Rev Cell Dev Biol 26: 115–136. https://doi.org/10.1146/annurev-cellbio-100109-104131
23. Ungermann C, Wickner W (1998) Vam7p, a vacuolar SNAP-25 homolog, is required for SNARE complex integrity and vacuole docking and fusion. EMBO J 17:3269–3276. https://doi.org/10.1093/emboj/17.12.3269
24. Cheever ML, Sato TK, de Beer T et al (2001) Phox domain interaction with PtdIns(3)P targets the Vam7 t-SNARE to vacuole membranes. Nat Cell Biol 3:613–618. https://doi.org/10.1038/35083000
25. Dulubova I, Sugita S, Hill S et al (1999) A conformational switch in syntaxin during exocytosis: role of munc18. EMBO J 18:4372–4382. https://doi.org/10.1093/emboj/18.16.4372
26. Sparks RP, Lawless W, Arango AS et al (2022) Use of microscale thermophoresis to measure protein-lipid interactions. J Vis Exp. https://doi.org/10.3791/60607
27. Kanai F, Liu H, Field SJ et al (2001) The PX domains of p47phox and p40phox bind to lipid products of PI(3)K. Nat Cell Biol 3:675–678. https://doi.org/10.1038/35083070
28. Stahelin RV, Long F, Diraviyam K et al (2002) Phosphatidylinositol 3-phosphate induces the membrane penetration of the FYVE domains of Vps27p and Hrs. J Biol Chem 277:26379–26388. https://doi.org/10.1074/jbc.M201106200
29. Chandra M, Chin YK-Y, Mas C et al (2019) Classification of the human phox homology (PX) domains based on their phosphoinositide binding specificities. Nat Commun 10:1528. https://doi.org/10.1038/s41467-019-09355-y
30. Lee SA, Kovacs J, Stahelin RV et al (2006) Molecular mechanism of membrane docking by the Vam7p PX domain. J Biol Chem 281: 37091–37101. https://doi.org/10.1074/jbc.M608610200

31. Weidman PJ, Melançon P, Block MR, Rothman JE (1989) Binding of an N-ethylmaleimide-sensitive fusion protein to Golgi membranes requires both a soluble protein(s) and an integral membrane receptor. J Cell Biol 108:1589–1596. https://doi.org/10.1083/jcb.108.5.1589
32. Wartchow CA, Podlaski F, Li S et al (2011) Biosensor-based small molecule fragment screening with biolayer interferometry. J Comput Aided Mol Des 25:669–676. https://doi.org/10.1007/s10822-011-9439-8
33. Wallner J, Lhota G, Jeschek D et al (2013) Application of bio-layer interferometry for the analysis of protein/liposome interactions. J Pharm Biomed Anal 72:150–154. https://doi.org/10.1016/j.jpba.2012.10.008
34. Petersen RL (2017) Strategies using bio-layer interferometry biosensor technology for vaccine research and development. Biosensors (Basel) 7:49. https://doi.org/10.3390/bios7040049
35. Shah NB, Duncan TM (2014) Bio-layer interferometry for measuring kinetics of protein-protein interactions and allosteric ligand effects. J Vis Exp e51383. https://doi.org/10.3791/51383
36. Fratti RA, Collins KM, Hickey CM, Wickner W (2007) Stringent 3Q.1R composition of the SNARE 0-layer can be bypassed for fusion by compensatory SNARE mutation or by lipid bilayer modification. J Biol Chem 282:14861–14867. https://doi.org/10.1074/jbc.M700971200
37. Fratti RA, Wickner W (2007) Distinct targeting and fusion functions of the PX and SNARE domains of yeast vacuolar Vam7p. J Biol Chem 282:13133–13138. https://doi.org/10.1074/jbc.M700584200